Chirality of Bloch domain walls in exchange-biased CoO/Co bilayer studied by waveguide-enhanced neutron spin-flip scattering

Yu. N. Khaydukov, D. Lenk, V. Zdravkov, Roman Morari, T. Keller, A. S. Sidorenko, L. R. Tagirov, R. Tidecks, Siegfried R. Horn, B. Keimer

Angaben zur Veröffentlichung / Publication details:

Khaydukov, Yu. N., D. Lenk, V. Zdravkov, Roman Morari, T. Keller, A. S. Sidorenko, L. R. Tagirov, R. Tidecks, Siegfried R. Horn, and B. Keimer. 2021. "Chirality of Bloch domain walls in exchange-biased CoO/Co bilayer studied by waveguide-enhanced neutron spin-flip scattering." *Physical Review B* 104 (17): 174445. https://doi.org/10.1103/physrevb.104.174445.

Chirality of Bloch domain walls in exchange-biased CoO/Co bilayer studied by waveguide-enhanced neutron spin-flip scattering

Yu. N. Khaydukov,[1,2,3] D. Lenk,[4] V. Zdravkov,[4,5] R. Morari,[4,5,6] T. Keller,[1,2] A. S. Sidorenko,[5,6] L. R. Tagirov,[4,7] R. Tidecks,[4] S. Horn,[4] and B. Keimer[1]

[1]*Max-Planck-Institut für Festkörperforschung, Heisenbergstraße 1, D-70569 Stuttgart, Germany*
[2]*Max Planck Society Outstation at the Heinz Maier-Leibnitz Zentrum (MLZ), D-85748 Garching, Germany*
[3]*Skobeltsyn Institute of Nuclear Physics, Moscow State University, Moscow 119991, Russia*
[4]*Institut für Physik, Universität Augsburg, D-86158 Augsburg, Germany*
[5]*Institute of Electronic Engineering and Nanotechnologies ASM, MD2028 Kishinev, Moldova*
[6]*Topological Quantum Phenomena in Superconducting Systems Lab (TQPSS), MIPT, Dolgoprudny, Russia*
[7]*Zavoisky Physical-Technical Institute, FRC Kazan Scientific Centre of RAS, 420029 Kazan, Russia*

(Received 15 July 2021; revised 8 November 2021; accepted 15 November 2021; published 30 November 2021)

The magnetic state of exchanged biased CoO(20 nm)/Co(d_F) bilayers ($d_F = 5-20$ nm) was studied by means of polarized neutron reflectometry. By introducing a Nb(20 nm) spacer layer between the CoO/Co bilayer and the Al_2O_3 substrate, we designed a resonator structure with significantly enhanced intensity of the spin-flip (SF) scattering at the position of the optical resonances. For the trained sample with thinnest Co layer ($d_F = 5$ nm), we detected strong SF scattering at the resonance position to the amount of 30% of the incoming intensity, pointing to a high degree of non-collinearity of the magnetization. With increasing d_F, the intensity of the SF scattering decreases linearly. Furthermore, an unconventional asymmetry of up-down and down-up scattering channels at the resonance positions was observed, which we ascribe to the out-of-plane magnetic stray field generated by chiral Bloch domain walls. This field leads to Zeeman splitting of the neutron energies depending on the initial neutron spin polarization. The chirality of the domain walls is assigned to the Dzyaloshinskii-Moriya interaction emerging at the CoO/Co interface. Our observations might prove useful for the design of spintronic devices based on the exchange bias effect.

DOI: 10.1103/PhysRevB.104.174445

I. INTRODUCTION

The exchange bias (EB) effect arises at the interface of antiferromagnetic (AF) and ferromagnetic (F) magnetic layers, and leads to a horizontal shift of the magnetic hysteresis loop by the exchange bias field H_{eb} (see review [1]). This effect was discovered 6 decades ago, and found widespread application in basic science [1,2], and in spintronic and superconducting devices taking advantage of the spin-valve effect [3–14].

Detailed characterization of EB thin film structures requires knowledge about the depth resolved and lateral magnetization profiles on a nm scale. The established method to measure these essential data is polarized neutron reflectometry (PNR) [15–31]. The raw data obtained by PNR are the spin-dependent neutron reflectivities $R^{\mu\nu}(Q)$, where $Q = 4\pi \sin\theta/\lambda$ is the momentum transfer, θ is the angle of incidence between neutron beam and film surface, and λ is the neutron wavelength. The indices μ, ν indicate the polarization of the incident and reflected neutron beams with respect to a quantization axis defined by an external field $\boldsymbol{H}$, where $+(-)$ label spin up (down) polarization. The non-spin-flip (NSF) reflectivities R^{++} and R^{--} are sensitive to the non-magnetic nuclear scattering length density (SLD) $\rho(z)$ of the system, and to the in-plane component $M_\parallel(z)$ of the magnetization parallel to $\boldsymbol{H}$: $R^{\pm\pm} \propto (\rho(z) \pm M_\parallel(z))$. For the analysis of $M_\parallel(z)$ it is convenient to define the spin asymmetry $S = (R^{++} - R^{--})/(R^{++} + R^{--})$, which is proportional to $M_\parallel(z)$. The noncollinear component of the magnetization $M_\perp(z)$ leads to spin-flip (SF) scattering: $R^{\pm\mp} \propto M_\perp(z)^2$. The depth resolved magnetization profiles $M_\parallel(z)$ and $M_\perp(z)$ and the nuclear SLD $\rho(z)$ are then obtained by a combined fit of a model potential to the four reflectivity curves $R^{\mu\nu}(Q)$. Such a fit requires knowledge of the sample structure and of the resolution properties of the neutron reflectometer. To resolve ambiguities in the reconstruction of the nuclear and magnetic profiles and to limit the number of potential models, additional data from complementary techniques, such as x-ray reflectometry and/or superconducting quantum interference device (SQUID) magnetometry, are required. There is a simple model-free method [17] to extract the angle α between the magnetization $\boldsymbol{M}$ and $\boldsymbol{H}$ (Fig. 1) from the measurement of the spin asymmetry in collinear case $S_{\rm sat}(\alpha = 0^\circ)$, and the SF reflectivity in fully noncollinear case $R^{\rm SF}_{\rm sat}(\alpha = 90^\circ)$:

$$S(\alpha)/S_{\rm sat}(0^\circ) = \cos(\alpha), \tag{1}$$

$$R^{\rm SF}(\alpha)/R^{\rm SF}_{\rm sat}(90^\circ) = \sin^2(\alpha). \tag{2}$$

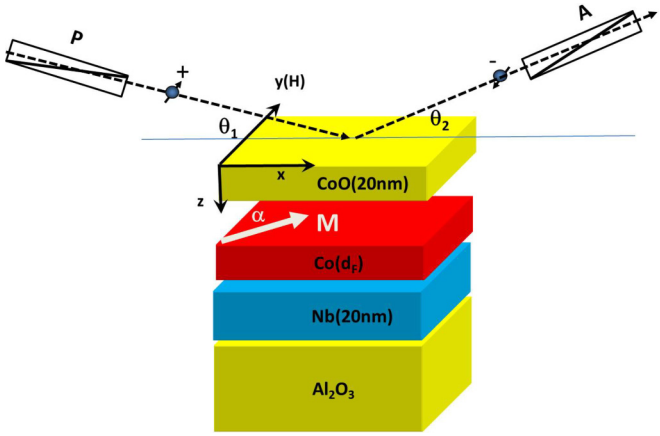

FIG. 1. Sketch of the PNR experiment, with Fe/Si supermirror transmission polarizer (P) and analyzer (A). Two spin-flippers up- and downstream the sample symbolically indicated by $+, -$ signs. The external field H is applied to the sample parallel to the y axis. α is the angle between the averaged magnetization $\boldsymbol{M}$ of the Co layer and $\boldsymbol{H}$.

Equations (1) and (2) are valid for arbitrary values of Q, but are limited to heterostructures containing only one F layer in a single domain state. For the multidomain state, there are two limiting cases, depending on the relation between the typical in-plane domain size ξ and neutron coherence length l_{coh}. *Large domains* with $\xi > l_{\text{coh}}$ will reflect the neutrons in the specular direction ($\theta_2 = \theta_1$), and the reflectivities of individual domains will be incoherently summed. For this case the statistical average of (1), (2) gives information about the so-called domains orientation dispersion σ^2:

$$\sigma^2 = \langle \cos^2(\alpha) \rangle - \langle \cos(\alpha) \rangle^2 = 1 - \langle \sin^2(\alpha) \rangle - \langle \cos(\alpha) \rangle^2. \quad (3)$$

Typical cases of Eq. (3) include a single domain ($\sigma^2 = 0$), domains with magnetization $\boldsymbol{M}$ collinear to $\boldsymbol{H}$ ($\sigma^2 = 1$), and domains with a dispersion of magnetic orientations ($0 < \sigma^2 < 1$). Domains with isotropic distribution of $\boldsymbol{M}$ correspond to $\sigma^2 = 0.5$. In the case of *small* domains with $\xi < l_{\text{coh}}$, neutrons will be scattered both in the specular and off-specular ($\theta_2 \neq \theta_1$) directions. The specular reflectivity then depends on the in-plane averaged $\langle \boldsymbol{M} \rangle$, which has a magnitude smaller then the saturated $\boldsymbol{M}$. Hence, expressions (1), (2) are not valid in this case, and the specular and off-specular reflectivity data have to be analyzed following the established conventional approaches [32,33].

For the study of magnetization reversal in EB systems, knowledge of the noncollinear part $M_\perp(z)$ extracted from the SF scattering is an essential parameter. The SF scattering is of purely magnetic origin with typically weak intensity, and the study of the magnetic properties of a single AF/F EB bilayer sample is usually strongly limited by counting statistics. A direct method to increase the SF signal intensity is to increase the sample volume by stacking a number of the identical bilayers [18,23–25,28]. This imposes two drawbacks: the roughness of the layers and hence the magnetic properties deteriorate with increasing number of layers, and the magnetic properties of a multilayer system might be quite different from the single bilayer. A second method to increase the SF signal intensity for a single bilayer is the waveguide or resonator technique. Here the bilayer is inserted between two layers with relatively high SLD forming a potential well. The neutron wave function forms resonances with enhanced intensity inside the resonator, i.e., inside the bilayer, such that also the SF intensity is resonantly enhanced. These resonant states occur for Q value below the critical edge Q_{crit} of total reflection. The waveguide requires a bespoke design to optimize the depth distribution of the neutron resonances with respect to the investigated EB bilayer. But there are sufficient degrees of freedom for the design. For example, instead of a potential well, neutron resonances also form at stair-step potentials.

For the study of EB the waveguide technique was first used by Radu *et al.* [19,20]. They used two additional relatively thick layers of Ti(200 nm) and Cu(100 nm) deposited on the sapphire substrate prior to deposition of EB Co(20 nm)/CoO(2.5 nm) bilayer. The intensity enhancement due to this resonator structure enabled a detailed study of magnetization reversal process of a single ferromagnetic film. We propose an alternative waveguide structure with improved quality resulting from a reduced number of deposited layers and a smaller layer thickness, namely CoO(20 nm)/Co(d_F)/Nb(20 nm)//Al_2O_3. We take advantage of the oxide substrate Al_2O_3 with high SLD ($\rho = 5.5 \times 10^{-4}\,\text{nm}^{-2}$) as the bottom layer of the waveguide, alternatively MgO ($\rho = 6 \times 10^{-4}\,\text{nm}^{-2}$) could be used. The high SLD of the oxides results from the large scattering length of the oxygen atoms. The oxide AF CoO of the EB bilayer forms the upper waveguide boundary layer with high SLD. Since a waveguide requires a minimum thickness of $\geqslant 10$ nm to form a neutron standing wave at the resonance condition, we introduced a Nb(20 nm) spacer layer in the design. Niobium is a superconductor with bulk transition temperature $T_C = 9.3$ K, so that the same structure can be used to study proximity effects at the superconducting/ferromagnet interface using PNR.

II. SAMPLE PREPARATION AND EXPERIMENTAL TECHNIQUES

Samples with nominal composition CoO(20 nm)/Co(d_F)/Nb(20 nm) were prepared by magnetron sputtering on a Leybold Z-400 machine, on Al_2O_3 substrates with $(1\bar{1}02)$ surface orientation (Fig. 1). Niobium and cobalt targets with purity of 99.99% were used, in an atmosphere of 8×10^{-3} mbar argon for the Nb and Co layers, and in Ar(83%) + O_2(17%) mixture of 9.6×10^{-3} mbar total pressure for the antiferromagnetic CoO layer formation. The purity of the Ar and O_2 gases was 99.999%, the residual pressure in the chamber was about 1.5×10^{-6} mbar. The targets and substrates were presputtered for 3–5 min to remove contaminations. The deposition rate was 4.5 nm/s for Nb, 0.1 nm/s for Co, and 0.08 nm/s for CoO. Samples for SQUID hysteresis loop measurements were prepared in wedge structures (procedure of the wedge deposition is described in Ref. [34]), with the thickness d_F of the Co layer varying in steps of $\delta d_F = 1.6$ nm in a range from 0 to 20 nm. For the neutron reflectometry we prepared four samples of size $10 \times 10\,\text{mm}^2$ with $d_F = 5$ nm (s05), 10 nm (s10), 15 nm (s15), and 20 nm (s20).

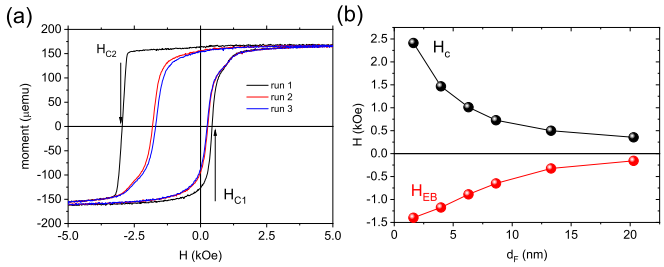

FIG. 2. (a) Hysteresis loops of the sample s05 ($d_F = 5.0\,\text{nm}$) at $T = 13\,\text{K}$ after cooling in $H = 4.5\,\text{kOe}$. The arrows show the positive and negative coercivity. (b) The d_F dependence of coercivity $H_c = (|H_{C1}| + |H_{C2}|)/2$ and the exchange bias field H_{eb}.

The neutron experiment was conducted at the monochromatic ($\lambda = 4.3\,\text{Å} \pm 2\%$) reflectometer NREX (MLZ, Garching) with horizontal sample alignment (Fig. 1). The beam divergence was $\delta\theta_z = 0.25\,\text{mrad}$ and $\delta\theta_y \sim 30\,\text{mrad}$ in the vertical and horizontal directions, respectively. From these values one can estimate [32] corresponding neutron coherence lengths of $l_{\text{coh,x}} \sim 10\,\mu\text{m}$ and $l_{\text{coh,y}} \sim 1\,\text{nm}$. The incident and the scattered beams were polarized with an efficiency of $P_P = 99.99(1)\%$ and analyzed with efficiency $P_A = 99.5(1)\%$ by Fe/Si supermirrors operated in transmission. The beam polarizations before and after the sample were defined by two adiabatic radio-frequency spin flippers with efficiencies close to 100%. An external magnetic field up to $H_{\text{max}} = 4.5\,\text{kOe}$ was applied to the sample in y direction, i.e., parallel to the surface and normal to the scattering plane.

For the reflectometry experiments, the samples were cooled down to $T = 13\,\text{K}$ in a closed cycle cryostat in He exchange gas. T is far below the blocking temperature $T_B = 180\,\text{K}$ of CoO and slightly above T_C of bulk Nb. Two different protocols were used to prepare the collinear (A) and noncollinear (B) states. (A) The sample was cooled in the maximum field of $H_{\text{max}} = 4.5\,\text{kOe}$ and trained by cycling three times through the hysteresis loop. As during the PNR experiment a negative external field at the sample would depolarize the neutron beam, we used for PNR at effective $H < 0$ the procedure outlined in prior work (see, for example, Ref. [18]), with cooling of the sample in negative magnetic field. (B) The noncollinear magnetic state with $\alpha = 90^\circ$ was obtained by cooling the sample in H_{max} to $T = 13\,\text{K}$ and then rotating the sample by 90° around the z axis with $H = 0$, such that the magnetization of the Co layer was aligned parallel to the x axis. Then for the PNR experiment $H \parallel y$ was applied.

III. EXPERIMENT

Figure 2(a) shows three successive hysteresis loops measured after cooling sample s05 in $H = 4.5\,\text{kOe}$ to $T = 13\,\text{K}$. The pristine loop shows sharp reversals at the coercive fields $H_{C1} = +0.4\,\text{kOe}$ and $H_{C2} = -3\,\text{kOe}$ with an exchange bias field $H_{eb} = (H_{C1} + H_{C2})/2 = -1.25\,\text{kOe}$. Subsequent field sweeps lead to a gradual decrease of H_{eb} with a stabilization of H_{eb} to $-0.7\,\text{kOe}$ after three loops, the so-called training effect. Figure 2(b) shows the coercive and exchange bias fields vs d_F in the trained state. The decrease of $H_{\text{eb}} \propto 1/d_F$ is a strong indication of the interfacial nature of the EB effect. The EB field $H_{\text{eb}} = -1.4\,\text{kOe}$ measured for the sample with the smallest $d_F = 1.6\,\text{nm}$ is one of the strongest EB effects observed thus far (see Table 3.1 in Ref. [1] for comparison).

Figures 3(a) and 3(b) show the spin-polarized reflectivity data for the samples s05 and s20 in the saturated state. Above the critical edge $Q > Q_{\text{crit}} = 0.16\,\text{nm}^{-1}$, the NSF reflectivities show a pronounced asymmetry. The SF reflectivities are zero within the statistical accuracy except for a small spin-leakage background (<1% of the NSF intensity) resulting from the efficiency ($P_P P_A < 1$) of the polarizer and analyzer. The experimental reflectivity data $R^{\mu\nu}(Q)$ were analyzed as described in our prior work [35–37] to extract nuclear and magnetic depth profiles. For both samples $R^{\mu\nu}(Q)$ are well described by the SLD depth profiles shown in panels Figs. 3(e) and 3(f), where the magnetization of the Co layer deviates only by 5% from Co bulk magnetization $4\pi M = 18\,\text{kG}$.

Figures 3(c) and 3(d) show reflectivity data for the samples s05 and s20 in the fully noncollinear state, obtained by protocol B. In this case the neutron reflectivity is characterized by zero spin asymmetry of the NSF channels and a pronounced SF scattering with one or two waveguide peaks $Q_{1,2}$ for the thin ($d_F < 15\,\text{nm}$) and thick ($d_F > 15\,\text{nm}$) samples, respectively. Using SLD profiles obtained from these reflectivity data, we calculated neutron density depth profiles $|\Psi(z)|^2$ at the Q values of the resonances [Figs. 3(e) and 3(f)]. The calculations show that for the samples with thin Co layer a resonant neutron standing wave forms at $Q = Q_1$, with maximum amplitude in the center of Nb layer [Fig. 3(e)]. The thick samples resonances at Q_1 and Q_2 correspond to neutron waves peaked at the centers of the Co and Nb layers, respectively [Fig. 3(f)]. Comparing samples s05 and s20, it is surprising that despite of the four times thinner Co layer of s05, the amplitude of the spin-flip reflectivity of 70% at the Q_1 resonance surpasses the reflectivity of 60% at Q_1 of the s20 sample. The reason is the higher amplitude of $|\Psi(z)|^2$ at the depth of the Co layer of s05, corresponding to a higher efficiency of waveguide enhancement of s05 compared to s20.

Figures 4(a) and 4(b) show the field dependence of the averaged cosine $\langle\cos\alpha\rangle$ (black) and squared-sine $\langle\sin^2\alpha\rangle$ (red) for the samples s05 and s20 (prepared by cooling protocol A) calculated from Eqs. (1), (2) using the data of Fig. 3 for normalization. To increase statistical accuracy for the calculation of $\langle\cos\alpha\rangle$, we integrated the spin-asymmetry S in the region of $Q_{\text{crit}} < Q < 0.2\,\text{nm}^{-1}$. For the calculation of $\langle\sin^2\alpha\rangle$ integrated the reflectivity R^{+-} and R^{-+} of the Q_1 peaks. This analysis shows that the magnetization reversal of s05 is characterized by a pronounced non-collinear state, with SF reflectivities as large as 30% and 20% in the vicinity of H_{C1} and H_{C2}. As shown in the inset of Fig. 4(a) the noncollinearity in the system appears due to the sample training.

Figures 4(c) and 4(f) show the SF reflectivities at the reversal points $H_{C1,2}$ for the samples s05 and s20. In contrast to the artificially created noncollinear state in Figs. 3(c) and 3(d), the SF reflectivities R^{+-} and R^{-+} are strongly different at the reversal points, except for H_{C1} of s05 [Fig. 4(c)]. For s05 we observe at H_{C2} a shift of $\Delta Q_1 = 8 \times 10^{-3}\,\text{nm}$ between the resonances for R^{+-} and R^{-+} [Fig. 4(e)], while for s20 only the R^{+-} peak was present at Q_1 for both H_{C1} and H_{C2}.

A similar asymmetry of the SF scattering was present not only at the reversal points but also in other fields with

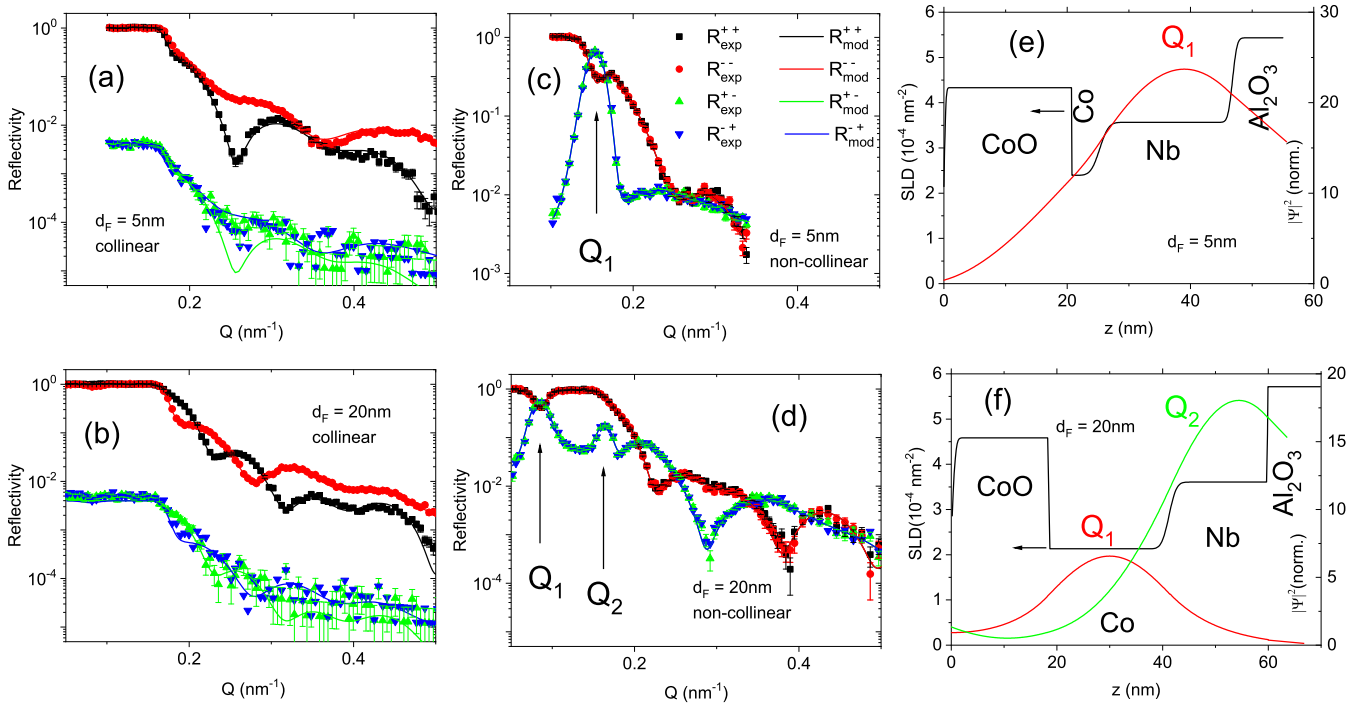

FIG. 3. PNR data and models in the saturated state. The collinear state prepared by cooling protocol A in the external field $H = 4.5$ kOe is shown in (a) for s05 ($d_F = 5$ nm) and (b) for s20 ($d_F = 20$ nm). The noncollinear state prepared by cooling protocol B in the external field $H = 5$ Oe is shown in (c) for s05 and (d) for s20. The solid lines in (a)–(d) correspond to best-fit model curves calculated for the SLD depth profiles depicted in (e) for s05 and (f) for s20. The vertical arrows in (c) and (d) indicate the positions of the resonance(s). The depth profile of neutron density at the resonances are shown in (e) and (f) by red and green lines.

a nonzero spin-flip signal. So Fig. 5 shows the SF curves measured for all samples in an external field of $H = 5$Oe (practically remanence). As can be seen, all samples with $d_F > 5$ nm show asymmetry of the SF channels.

IV. DISCUSSION AND CONCLUSION

In this work we systematically studied the magnetization reversal of the EB bilayers CoO(20 nm)/Co(d_F) with $d_F = 5-20$ nm by means of waveguide-enhanced neutron SF scattering. The trained samples are characterized by pronounced and robust SF scattering. We relate this SF scattering to the presence of a domain state previously observed in CoO/Co systems by various microscopic methods [38,39]. The analysis of all polarization channels and the d_F dependence provides detailed information about the magnetization reversal mechanism. Sample s05 with a thin Co layer ($d_F = 5$ nm) is characterized by a high SF reflectivity reaching a level of 20–30% near the reversal points $H_{C1,2}$. With Eq. (3) we estimate $\sigma^2 \sim 0.5$, which indicates that the thin cobalt film is remagnetized through fragmentation to fairly isotropically oriented magnetic domains. Increasing d_F leads to a linear decrease of the SF intensity to 2% for $d_F = 20$ nm, so that $\sigma^2 \sim 1$ at the reversal points. This corresponds to the situation of collinear domains, and the remagnetization through a movement of the domain wall.

A prominent feature in the present data is the inequality of the R^{+-} and R^{-+} reflectivities. Such an asymmetry of the SF signal of PNR data is a rather exotic phenomenon. It was previously observed in elastic neutron diffraction on helimagnets [40–45] or in inelastic neutron scattering by magnons in bulk systems [46]. In a preceding PNR experiment on a CoO(2.5nm)/Co(20nm) EB bilayer, a similar shift of the SF waveguide peaks was reported. The authors argued that this peak shift can be explained by Zeeman splitting of the energies of the incident spin-up and spin-down neutrons [19]. The effect was observed in the spin-flip scattering channels at relatively high external magnetic fields (order of kOe) [47–52].

In order to show experimentally that the peak shift observed in our measurements is related to an external field rather than an internal magnetic state of the Co layer, we measured the H dependence of the SF channels R^{+-} and R^{-+} of pristine samples in the noncollinear state prepared by protocol B. In this experiment, we did not change the direction (sign) of the external field, so we can assume that the internal magnetic domain state of the Co layer remained independent of H. Figures 6(a) and 6(b) show the data for the samples s05 ($H = 1.4$ kOe) and s20 ($H = 300$ Oe), where H is chosen to be close to H_{C2}. We observe a splitting of the R^{+-} and R^{-+} reflectivities, which gives strong evidence that the asymmetry of the SF scattering is related to the external magnetic field. The splitting grows linearly with H, such that $\Delta Q_1 = c \times H$ [insets in Figs. 6(a) and 6(b)]. For the samples s05, s15, and s20, we obtained the slopes $c = 5.4$, 6.3, and 10.5, respectively (unit: 1×10^{-6} nm$^{-1}Oe^{-1}$). The peak splitting ΔQ_1 observed for sample s05 in Fig. 6(a) at $H = 1.4$ kOe is identical to the splitting observed for s05 at H_{C2} [Fig. 4(e)]. As the sample was prepared by different cooling protocols in these two measurements and thus

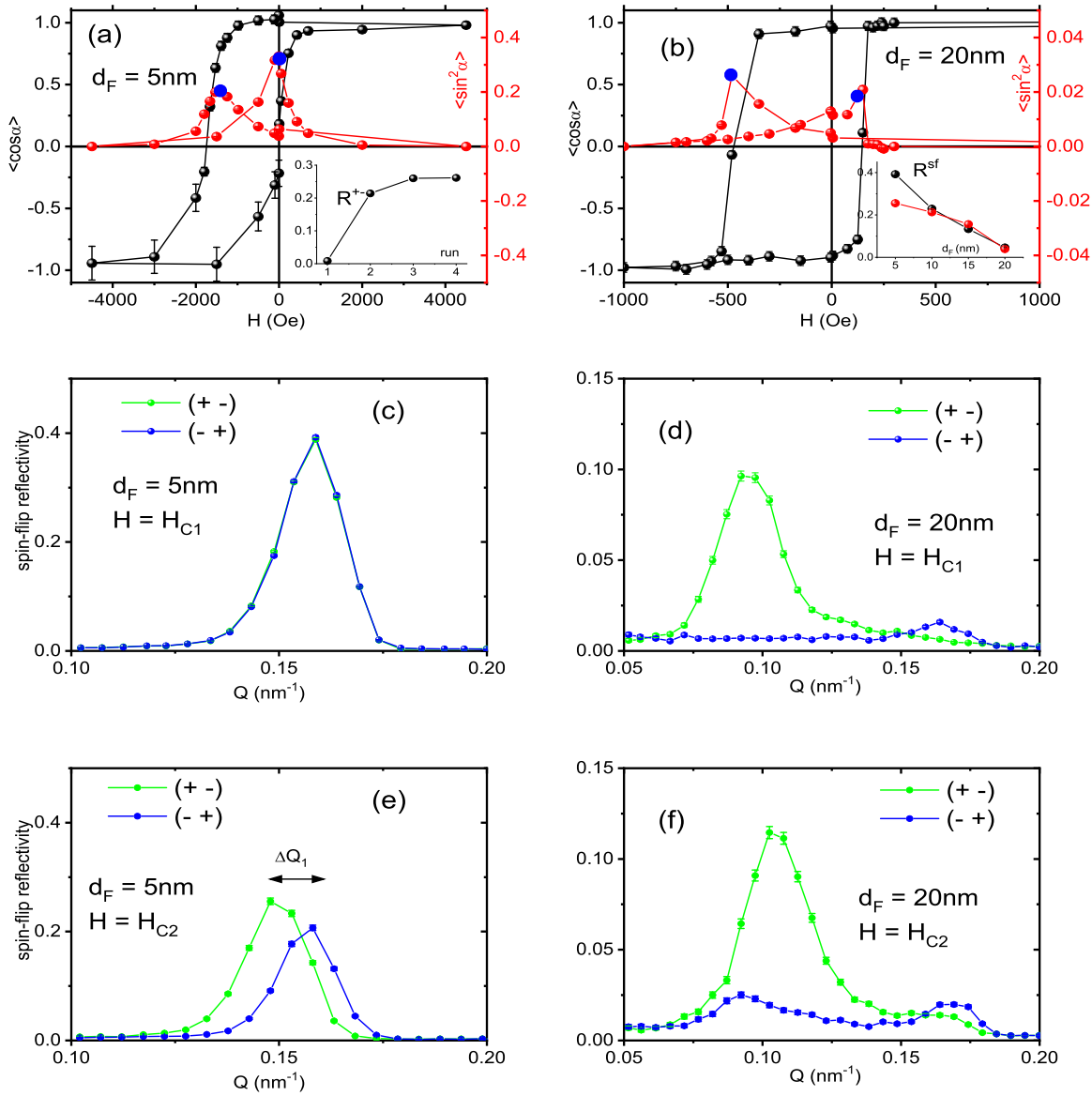

FIG. 4. The field dependence of the normalized spin asymmetry and spin-flip scattering for the sample (a) s05 and (b) s20 prepared by cooling protocol A. $\langle \sin^2 \alpha \rangle$ in (a) and (b) differ by one order of magnitude. The inset in (a) shows the amplitude of spin-flip peak at Q_1 resonance at H_{C1} versus the number of field cycles. The inset in (b) shows the amplitude of the spin-flip peak at H_{C1} (black) and H_{C2} (red) as a function of d_F. Panels (c), (e) and (d), (f) show spin-flip reflectivity measured in the vicinity of H_{C1} and H_{C2} [depicted by blue circles in (a) and (b)] for the samples s05 and s20, respectively. The horizontal arrow in (e) depicts the peak splitting ΔQ_1.

had different domain states, the splitting can entirely be explained by the external field, rather than by the domain state.

For the other samples, however, the applied magnetic field cannot quantitatively explain the observed asymmetry of the SF scattering. For instance, for s10 at $H = 5\,\mathrm{Oe}$

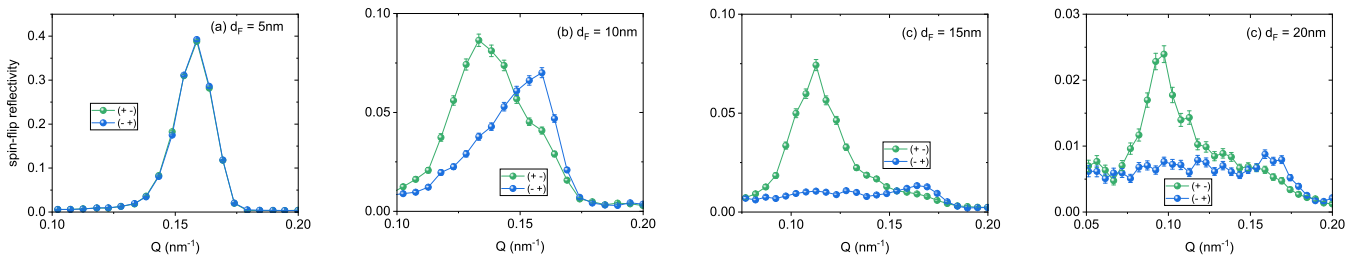

FIG. 5. SF reflectivity R^{+-} and R^{-+} measured in magnetic field $H = 5\,\mathrm{Oe}$ after cooling the samples in protocol A, training, and magnetization in negative field.

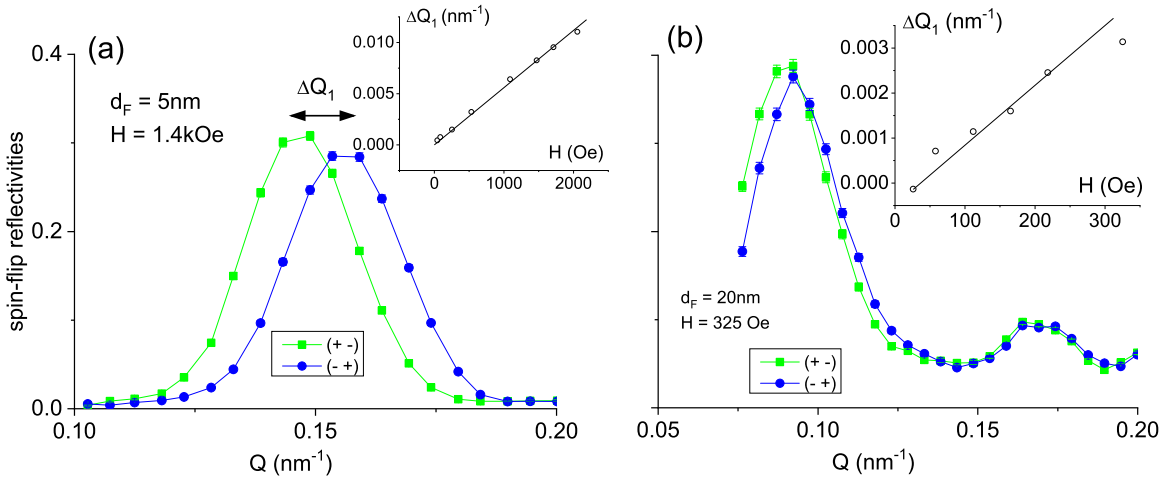

FIG. 6. SF reflectivity R^{+-} and R^{-+} measured (a) on pristine sample s05 in the $H = 1.4$ kOe and (b) on a pristine sample s20 in $H = 325$ Oe. H was applied perpendicular to the field direction during cooling. The insets show the peak shift ΔQ_1 vs H.

(almost remanence) the first resonant peak was split by $\Delta Q_1 = 0.02\,\text{nm}^{-1}$. This splitting would correspond to $H \sim 3$ kOe. For the samples s15 and s20 with increased Co layer thickness, the resonance was only observed in the R^{+-} channel, and was absent in the R^{-+} channel [Figs. 4(d) and 5(f)]. We can assume that this absent resonance was shifted below the experimental minimum $Q = 0.05\,\text{nm}^{-1}$. Thus, we estimate $\Delta Q_1 > 0.03\,\text{nm}^{-1}$, corresponding to $H \sim 5$ kOe.

The aforementioned observations lead us to the conclusion that for the samples with $d_F > 5$ nm, the splitting of the resonance peaks can be explained by an external field significantly exceeding the H applied by the electromagnet. Following Radu et *al.* [19], we conclude that the additional field is generated by out-of-plane stray fields of the Bloch domain walls. Indeed, it is a well-known fact that thin magnetic layers, due to the strong shape anisotropy, are characterized by the in-plane Neel domain walls. These in-plane domain walls will not produce any out-of-plane stray field. This is the case for the thin Co(5nm) layer. With increasing d_F, the shape anisotropy energy decreases, and Bloch domain walls with out-of-plane magnetization components become energetically preferable. These Bloch domain walls can generate a stray field outside the film. For equally populated left- and right handed rotating Bloch walls these stray fields average to zero. However, if there is chirality present, this means an unequal population of the Bloch domain wall rotational handedness, a net external stray field persists.

Chiral domains have indeed been observed by direct microscopic methods in Fe/Ni/Cu [53] and Co/Pd [54] systems with strong perpendicular magnetic anisotropy (PMA). For these systems the interfacial Dzyaloshinskii-Moriya Interaction (DMI) was identified to be responsible for breaking the degeneracy of Bloch chiralities. The direct observation of the DMI in PMA Pt/Co/Ni system by means of Brillouin spectroscopy (BS) was also reported in Ref. [55]. As to the EB systems, the same Brillouin spectroscopy helped to establish the presence of the interfacial DMI on the interface between antiferromagnetic IrMn and feromagnetic CoFeB. In this regard, it seems reasonable to assume that the same DMI may cause the chirality of the Bloch domain walls and in our exchange-biased CoO/Co systems. Nevertheless, a more affirmative answer can be obtained from magnetic microscopic and BS experiments that will be reported elsewhere. The usefulness of the waveguide-enhanced PNR experiments in this case consists of the possibility of accurate measurement of the cumulative out-of-plane magnetic field created by chiral Bloch walls. For this, however, further development of modern freely available fitting software, such as genX [56] or ESCAPE [57] is required.

In summary, we systematically studied the d_F-dependence of the magnetic state of exchange biased CoO(20nm)/Co(d_F) bilayers ($d_F = 5-20$ nm) by means of waveguide-enhanced polarized neutron reflectometry. The design of the waveguide structure proposed in this work takes advantage of the high scattering power of oxides, which allows to use the antiferromagnetic CoO layer as a part of the waveguide design, thus improving the quality of the structure. Our investigation shows that the magnetization reversal of the exchanged-biased CoO/Co bilayer significantly depends on the thickness of the cobalt layer. The systems with $d_F > 5$ nm are re-magnetized through the motion of chiral Bloch domain walls. The chirality of these walls leads to the emergence of out-of-plane magnetic stray fields of several kOe. In the PNR experiment, these stray fields lead to an asymmetry of the spin-flip reflectivities at the waveguide resonances. The analysis method of resonant spin-flip scattering asymmetry developed in this work can provide useful parameters for spintronics applications, namely for the design of spin-valve systems with a controllable level of noncollinearity and noncoplanarity. In addition, our waveguide design with a superconducting spacer allows to study triplet superconducting spin valves [3].

ACKNOWLEDGMENTS

We would like to thank T. Saerback, B. Toperverg, V. Bodnarchuk, O. Udalov, S. Kozhevnikov, M. Fitzsimmons, and A. Devishvili for the fruitful discussions. We also express our gratitude to F. Tralmer for his technical support. This work is based upon experiments performed at the NREX instrument operated by Max-Planck Society at the

Heinz Maier-Leibnitz Zentrum (MLZ), Garching, Germany and supported by German Research Foundation (Deutsche Forschungsgemeinschaft, DFG, Project No. 107745057 - TRR80). A.S.S. and R.M. thank the support of the "SPINTECH" project of the HORIZON-2020 TWINNING program (2018-2020). R.M. is also grateful for the support from the Russian Ministry of Education and Science within the program 5top100. L.R.T. acknowledges the support from the Ministry of Education and Science of the Russian Federation in the frame of Agreement No. 075-15-2021-623 with the FRC Kazan Scientific Centre of RAS. Y.N.K. acknowledges the support from Russian Ministry of Science and Education Grant No. 075-15-2021-1353 (development of the neutron standing wave method).

[1] F. Radu and H. Zabel, Exchange bias effect of ferro-/antiferromagnetic heterostructures, in *Magnetic Heterostructures: Advances and Perspectives in Spinstructures and Spintransport*, edited by H. Zabel and S. D. Bader (Springer, Berlin, 2008), p. 97.

[2] Z. Liu, Recent advances in exchange bias of layered magnetic FM/AFM systems, Sci. Chin. Phys. Mech. **56**, 61 (2012).

[3] L. R. Tagirov, M. Y. Kupriyanov, V. N. Kushnir, and A. Sidorenko, Superconducting triplet proximity and Josephson spin valves, in *NanoScience and Technology* (Springer International Publishing, New York, 2018), p. 31.

[4] V. N. Kushnir, A. Sidorenko, L. R. Tagirov, and M. Y. Kupriyanov, Basic superconducting spin valves, in *NanoScience and Technology* (Springer International Publishing, New York, 2018), p. 1.

[5] D. Lenk, R. Morari, V. I. Zdravkov, A. Ullrich, Y. Khaydukov, G. Obermeier, C. Müller, A. S. Sidorenko, H.-A. K. von Nidda, S. Horn, L. R. Tagirov, and R. Tidecks, Full-switching FSF-type superconducting spin-triplet magnetic random access memory element, Phys. Rev. B **96**, 184521 (2017).

[6] P. V. Leksin, A. A. Kamashev, J. Schumann, V. E. Kataev, J. Thomas, B. Büchner, and I. A. Garifullin, Boosting the superconducting spin valve effect in a metallic superconductor/ferromagnet heterostructure, Nano Res. **9**, 1005 (2016).

[7] D. Lenk, V. I. Zdravkov, J.-M. Kehrle, G. Obermeier, A. Ullrich, R. Morari, H.-A. K. von Nidda, C. Müller, M. Y. Kupriyanov, A. S. Sidorenko, S. Horn, R. G. Deminov, L. R. Tagirov, and R. Tidecks, Thickness dependence of the triplet spin-valve effect in superconductor–ferromagnet–ferromagnet heterostructures, Beilstein J. Nanotechnol. **7**, 957 (2016).

[8] D. Stamopoulos, E. Aristomenopoulou, and E. Manios, Absolute supercurrent switch in ferromagnetic/superconducting/ferromagnetic trilayers operating at T >4.2 K, Appl. Phys. Lett. **105**, 112602 (2014).

[9] N. Banerjee, C. B. Smiet, R. G. J. Smits, A. Ozaeta, F. S. Bergeret, M. G. Blamire, and J. W. A. Robinson, Evidence for spin selectivity of triplet pairs in superconducting spin valves, Nat. Commun. **5**, 3048 (2014).

[10] M. G. Flokstra, T. C. Cunningham, J. Kim, N. Satchell, G. Burnell, P. J. Curran, S. J. Bending, C. J. Kinane, J. F. K. Cooper, S. Langridge, A. Isidori, N. Pugach, M. Eschrig, and S. L. Lee, Controlled suppression of superconductivity by the generation of polarized Cooper pairs in spin-valve structures, Phys. Rev. B **91**, 060501(R) (2015).

[11] V. I. Zdravkov, D. Lenk, R. Morari, A. Ullrich, G. Obermeier, C. Müller, H.-A. K. von Nidda, A. S. Sidorenko, S. Horn, R. Tidecks, and L. R. Tagirov, Memory effect and triplet pairing generation in the superconducting exchange biased co/CoOx/$Cu_{41}Ni_{59}$/Nb/$Cu_{41}Ni_{59}$ layered heterostructure, Appl. Phys. Lett. **103**, 062604 (2013).

[12] V. I. Zdravkov, J. Kehrle, G. Obermeier, D. Lenk, H.-A. von Nidda, C. Müller, M. Y. Kupriyanov, A. S. Sidorenko, S. Horn, R. Tidecks, and L. R. Tagirov, Experimental observation of the triplet spin-valve effect in a superconductor-ferromagnet heterostructure, Phys. Rev. B **87**, 144507 (2013).

[13] P. V. Leksin, N. N. Garif'yanov, I. A. Garifullin, J. Schumann, V. Kataev, O. G. Schmidt, and B. Büchner, Physical properties of the superconducting spin-valve Fe/Cu/Fe/In heterostructure, Phys. Rev. B **85**, 024502 (2012).

[14] P. V. Leksin, N. N. Garif'yanov, I. A. Garifullin, Y. V. Fominov, J. Schumann, Y. Krupskaya, V. Kataev, O. G. Schmidt, and B. Büchner, Evidence for Triplet Superconductivity in a Superconductor-Ferromagnet Spin Valve, Phys. Rev. Lett. **109**, 057005 (2012).

[15] M. R. Fitzsimmons, P. Yashar, C. Leighton, I. K. Schuller, J. Nogués, C. F. Majkrzak, and J. A. Dura, Asymmetric Magnetization Reversal in Exchange-Biased Hysteresis Loops, Phys. Rev. Lett. **84**, 3986 (2000).

[16] C. Leighton, M. R. Fitzsimmons, P. Yashar, A. Hoffmann, J. Nogués, J. Dura, C. F. Majkrzak, and I. K. Schuller, Two-Stage Magnetization Reversal in Exchange Biased Bilayers, Phys. Rev. Lett. **86**, 4394 (2001).

[17] W.-T. Lee, S. G. E. te Velthuis, G. P. Felcher, F. Klose, T. Gredig, and E. D. Dahlberg, Ferromagnetic domain distribution in thin films during magnetization reversal, Phys. Rev. B **65**, 224417 (2002).

[18] F. Radu, M. Etzkorn, V. Leiner, T. Schmitte, A. Schreyer, K. Westerholt, and H. Zabel, Polarised neutron reflectometry study of Co/CoO exchange-biased multilayers, Appl. Phys. A **74**, s1570 (2002).

[19] F. Radu, A. Vorobiev, J. Major, H. Humblot, K. Westerholt, and H. Zabel, Spin-resolved off-specular neutron scattering from magnetic domain walls using the polarized 3He gas spin filter, Physica B **335**, 63 (2003).

[20] F. Radu, M. Etzkorn, R. Siebrecht, T. Schmitte, K. Westerholt, and H. Zabel, Interfacial domain formation during magnetization reversal in exchange-biased CoO/Co bilayers, Phys. Rev. B **67**, 134409 (2003).

[21] F. Radu, A. Westphalen, K. Theis-Bröhl, and H. Zabel, Quantitative description of the azimuthal dependence of the exchange bias effect, J. Phys.: Condens. Matter **18**, L29 (2005).

[22] A. Paul, E. Kentzinger, U. Rücker, and T. Brückel, The angular dependence of the magnetization reversal in exchange biased multilayers, J. Condens. Matter Phys. **18**, L149 (2006).

[23] A. Paul, E. Kentzinger, U. Rücker, and T. Brückel, Magnetization reversal with variation of the ratio of the anisotropy

energies in exchange bias systems, Phys. Rev. B **74**, 054424 (2006).

[24] A. Paul, T. Brückel, E. Kentzinger, and U. Rücker, Magnetization reversal in trained exchange biased multilayers, J. Condens. Matter Phys. **19**, 086229 (2007).

[25] A. Paul and S. Mattauch, Can uniaxial anisotropy be responsible for training in exchange coupled system? J. Appl. Phys. **108**, 053918 (2010).

[26] D. L. Cortie, K.-W. Lin, C. Shueh, H.-F. Hsu, X. L. Wang, M. James, H. Fritzsche, S. Brück, and F. Klose, Exchange bias in a nanocrystalline hematite/permalloy thin film investigated with polarized neutron reflectometry, Phys. Rev. B **86**, 054408 (2012).

[27] J. Demeter, E. Menéndez, A. Teichert, R. Steitz, D. Paramanik, C. V. Haesendonck, A. Vantomme, and K. Temst, Influence of magnetocrystalline anisotropy on the magnetization reversal mechanism in exchange bias Co/CoO bilayers, Solid State Commun. **152**, 292 (2012).

[28] A. Paul, N. Paul, J. Jutimoosik, R. Yimnirun, S. Rujirawat, B. Höpfner, I. Lauermann, M. Lux-Steiner, S. Mattauch, and P. Böni, Change in interface magnetism of an exchange-coupled system due to the presence of nonmagnetic spacers, Phys. Rev. B **87**, 014431 (2013).

[29] Y. Khaydukov, R. Morari, V. Zdravkov, L. Mustafa, T. Keller, B. Keimer, and A. Sidorenko, Evolution of noncollinear magnetic state of exchange biased ferromagnet/normal metal/ferromagnet/superconductor heterostructure in magnetic field studied by polarized neutron reflectometry, Low Temp. Phys. **43**, 837 (2017).

[30] G. Kim, Y. Khaydukov, M. Bluschke, Y. E. Suyolcu, G. Christiani, K. Son, C. Dietl, T. Keller, E. Weschke, P. A. van Aken, G. Logvenov, and B. Keimer, Tunable perpendicular exchange bias in oxide heterostructures, Phys. Rev. Mater. **3**, 084420 (2019).

[31] K. Chen, A. Philippi-Kobs, V. Lauter, A. Vorobiev, E. Dyadkina, V. Y. Yakovchuk, S. Stolyar, and D. Lott, Observation of a chirality-induced exchange-bias effect, Phys. Rev. Appl. **12**, 024047 (2019).

[32] H. Zabel, K. Theis-Bröhl, and B. P. Toperverg, Polarized neutron reflectivity and scattering from magnetic nanostructures and spintronic materials, in *Handbook of Magnetism and Advanced Magnetic Materials* (American Cancer Society, Atlanta, GA, 2007).

[33] B. P. Toperverg, Polarized neutron reflectometry of magnetic nanostructures, Phys. Met. Metallogr. **116**, 1337 (2015).

[34] A. Sidorenko, V. Zdravkov, A. Prepelitsa, C. Helbig, Y. Luo, S. Gsell, M. Schreck, S. Klimm, S. Horn, L. Tagirov, and R. Tidecks, Oscillations of the critical temperature in superconducting Nb/Ni bilayers, Ann. Phys. **12**, 37 (2003).

[35] Y. N. Khaydukov, G. A. Ovsyannikov, A. E. Sheyerman, K. Y. Constantinian, L. Mustafa, T. Keller, M. A. Uribe-Laverde, Y. V. Kislinskii, A. V. Shadrin, A. Kalaboukhov, B. Keimer, and D. Winkler, Evidence for spin-triplet superconducting correlations in metal-oxide heterostructures with noncollinear magnetization, Phys. Rev. B **90**, 035130 (2014).

[36] Y. Khaydukov, A. M. Petrzhik, I. V. Borisenko, A. Kalabukhov, D. Winkler, T. Keller, G. A. Ovsyannikov, and B. Keimer, Magnetic waveguides for neutron reflectometry, Phys. Rev. B **96**, 165414 (2017).

[37] Y. N. Khaydukov, E. A. Kravtsov, V. D. Zhaketov, V. V. Progliado, G. Kim, Y. V. Nikitenko, T. Keller, V. V. Ustinov, V. L. Aksenov, and B. Keimer, Magnetic proximity effect in Nb/Gd superlattices seen by neutron reflectometry, Phys. Rev. B **99**, 140503(R) (2019).

[38] U. Welp, S. G. E. te Velthuis, G. P. Felcher, T. Gredig, and E. D. Dahlberg, Domain formation in exchange biased Co/CoO bilayers, J. Appl. Phys. **93**, 7726 (2003).

[39] S. Brems, A. Volodin, C. V. Haesendonck, and K. Temst, Magnetic force microscopy study of the training effect in polycrystalline Co/CoO bilayers, J. Appl. Phys. **103**, 113912 (2008).

[40] C. Schwink and O. Schärpf, Solution of the Pauli equation for neutrons in varying magnetic fields and its application to reflection and transmission at helical magnetic structures, Z. Phys. **21**, 305 (1975).

[41] V. L. Aksenov, V. K. Ignatovich, and Y. V. Nikitenko, Reflection of neutrons from a helical system, JETP Lett. **84**, 473 (2007).

[42] A. A. Fraerman and O. G. Udalov, Specific features of the motion of neutrons in a medium with a helical magnetic structure, J. Exp. Theor **104**, 62 (2007).

[43] S. V. Grigoriev, Y. O. Chetverikov, D. Lott, and A. Schreyer, Field Induced Chirality in the Helix Structure of Dy/Y Multilayer Films and Experimental Evidence for Dzyaloshinskii-Moriya Interaction on the Interfaces, Phys. Rev. Lett. **100**, 197203 (2008).

[44] V. V. Tarnavich, D. Lott, S. Mattauch, A. Oleshkevych, V. Kapaklis, and S. V. Grigoriev, Field-induced chirality in the helix structure of Ho/Y multilayers, Phys. Rev. B **89**, 054406 (2014).

[45] V. Tarnavich, E. Tartakovskaya, Y. Chetverikov, V. Golub, D. Lott, Y. Chernenkov, A. Devishvili, V. Ukleev, V. Kapaklis, A. Oleshkevych, V. Fedorov, V. Bairamukov, A. Vorobiev, and S. Grigoriev, Magnetic field induced chirality in Ho/Y multilayers with gradually decreasing anisotropy, Phys. Rev. B **96**, 014415 (2017).

[46] A. Gukasov, Left–right asymmetry in polarised neutron scattering, Physica B **267**, 97 (1999).

[47] G. Felcher, S. Adenwalla, V. De Haan, and A. Van Well, Zeeman splitting of surface-scattered neutrons, Nature (London) **377**, 409 (1995).

[48] V. Aksenov, Y. Nikitenko, and S. Kozhevnikov, Spin-flip spatial neutron beam splitting in magnetic media, Physica B **297**, 94 (2001).

[49] S. Kozhevnikov, F. Ott, and F. Radu, Data representations of Zeeman spatial beam splitting in polarized neutron reflectometry, J. Appl. Crystallogr. **45**, 814 (2012).

[50] B. B. Maranville, B. J. Kirby, A. J. Grutter, P. A. Kienzle, C. F. Majkrzak, Y. Liu, and C. L. Dennis, Measurement and modeling of polarized specular neutron reflectivity in large magnetic fields, J. of Appl. Crystallogr. **49**, 1121 (2016).

[51] S. Kozhevnikov, F. Ott, and E. Semenova, Neutron Zeeman beam-splitting for the investigation of magnetic nanostructures, Physica B **508**, 12 (2017).

[52] S. V. Kozhevnikov, V. K. Ignatovich, and F. Radu, On the application of Zeeman spatial beam splitting in polarized neutron reflectometry, J. Surf. Invest.: X-Ray, Synchrotron Neutron Tech. **12**, 103 (2018).

[53] G. Chen, J. Zhu, A. Quesada, J. Li, A. T. N'Diaye, Y. Huo, T. P. Ma, Y. Chen, H. Y. Kwon, C. Won, Z. Q. Qiu, A. K. Schmid, and Y. Z. Wu, Novel Chiral Magnetic Domain wall Structure in Fe/Ni/Cu(001) Films, Phys. Rev. Lett. **110**, 177204 (2013).

[54] S. D. Pollard, J. A. Garlow, K.-W. Kim, S. Cheng, K. Cai, Y. Zhu, and H. Yang, Bloch Chirality Induced by an Interlayer Dzyaloshinskii-Moriya Interaction in Ferromagnetic Multilayers, Phys. Rev. Lett. **125**, 227203 (2020).

[55] K. Di, V. L. Zhang, H. S. Lim, S. C. Ng, M. H. Kuok, J. Yu, J. Yoon, X. Qiu, and H. Yang, Direct Observation of the Dzyaloshinskii-Moriya Interaction in a Pt/Co/Ni Film, Phys. Rev. Lett. **114**, 047201 (2015).

[56] M. Björck and G. Andersson, GenX: An extensible x-ray reflectivity refinement program utilizing differential evolution, J. Appl. Crystallogr. **40**, 1174 (2007).

[57] D. Korolkov and S. Rakhimov, Essential scattering applications for everyone. overview (2020), arXiv:2011.01340.